Striated microdischarges in an asymmetric barrier discharge in argon at atmospheric pressure

Tomáš Hoder,* Detlef Loffhagen,† Christian Wilke, Helge Grosch, Jan Schäfer, Klaus-Dieter Weltmann, and Ronny Brandenburg

Leibniz Institute for Plasma Science and Technology, Felix-Hausdorff-Str. 2, D-17489 Greifswald, Germany

(Received 16 June 2010; revised manuscript received 19 July 2011; published 17 October 2011)

The investigation of striated microdischarges in barrier discharges in argon at atmospheric pressure is reported. Microdischarges were investigated by means of electrical measurements correlated with intensified CCD camera imaging. The scaling law theory known from low-pressure glow discharge diagnostics was applied in order to describe and explain this phenomenon. The investigated microdischarge is characterized as a transient atmospheric-pressure glow discharge with a stratified column. It can be described by similarity parameters $i/r \approx 0.13$ A/cm, $pr \approx 5$ Torr cm, and $3 < \lambda/r < 5$ with the current i, pressure p, interval of subsequent striations λ, and radius of the plasma channel r. An attempt to describe the mechanism of creation of a striated structure is given, based on an established model of the spatial electron relaxation.

DOI: 10.1103/PhysRevE.84.046404 PACS number(s): 52.35.Mw, 52.70.Kz, 52.80.Hc

I. INTRODUCTION

The appearance of striated structures in glow discharges at low and medium pressure is well known and has been reviewed in many publications [1–6]. Recently, these structures have also been observed at atmospheric pressure in glow discharges [7–9], microwave excited discharges [10], hollow cathode plasmas [11], and plasma jets [12,13]. In particular, the longitudinal stratification of filaments in an atmospheric-pressure rf plasma jet in argon has been detected in relation to a self-organization effect in Ref. [13].

The stability and reproducibility of the plasma is crucial for its industrial application and the understanding of striated structures is one aspect to be clarified to produce convenient and well-defined plasmas. Frequently, the striated structure within the plasma channel at low pressure appears as a result of a relaxation process induced by a local disturbance, which can be caused, for example, by a probe, a short laser pulse, or a discharge constriction [14–17]. However, these instabilities are not yet fully understood for atmospheric-pressure plasmas, which have been the subject of extensive research in the last decade [18]. For example, varying the discharge parameters (e.g., the applied voltage between electrodes), a sequence of state transitions is frequently observed [19]. Periodical and irregular states follow each other. The transitions of these states were reached by even very small changes of the parameter. Due to their nonlinear nature, they are direction dependent and show a hysteresis in their behavior [20–24].

In this paper the observation of striated microdischarges in asymmetric argon barrier discharges at atmospheric pressure is reported. Typical pictures of striated microdischarges are shown in Fig. 1 (note that the subscript p-p in the units $kV_{p\text{-}p}$ refers to "peak to peak"). The appearance of the striated structure is not related to the presence of the metallic electrode in asymmetric barrier discharge arrangements, where one electrode is covered by a dielectric. Indeed, in the case of symmetric barrier discharges, where both electrodes are covered by a dielectric, the striated structure has been found as well. However, the appearance of striated microdischarges in the symmetric setup was rare and instable. As can be seen in Fig. 1, the striated structures appear not only within the discharge channel in the gap, but also directly on the surface of the electrodes. Striated structures have been observed for both polarities in asymmetric barrier discharges; that is, for the arrangement with metallic cathode and dielectric-covered anode (M−D+) as well as with metallic anode and dielectric cathode (M+D−). However, they were too unstable for more detailed research in the M+D− arrangement. The irreproducibility of this discharge can be caused by the inhomogeneous deposition of the surface charges onto the dielectric surfaces in the barrier discharge setup. This phenomenon was described in [25,26].

In order to gain better knowledge of the discharge behavior, experimental studies have been performed, consisting of electrical measurements which were correlated with imaging of the discharge plasma by means of an intensified CCD camera. The main features of the experiments are given. The development of striated microdischarges is described in detail, and a discussion of the mechanisms of the discharge creation is presented. In addition, the striated discharge has been analyzed by means of similarity parameters according to the scaling law theory given in [27,28] and by solving the inhomogeneous Boltzmann equation of the electrons for a spatially periodic electric field typical of striations.

II. EXPERIMENTAL SETUP

The discharge cell used for the investigations is shown in Fig. 2. Electrodes were placed into an acrylic glass chamber with the volume of 4 cm^3. The mutual distance of the pure metal (stainless steel) and alumina-covered electrode was 1.5 mm. The thickness of the dielectric was 1 mm. The curvature of both electrode tips was 2 mm. The metal electrode was energized by high voltage and the other electrode was grounded.

The barrier discharge was generated at atmospheric pressure by a 60 kHz sinusoidal voltage. A Softal AT6003 transformer, QSC Powerlight 9.0 PFC amplifier, and Toellner TOE 7711A function generator were used. The voltage and current characteristics were measured by Tektronix probes

*hoder@inp-greifswald.de
†loffhagen@inp-greifswald.de

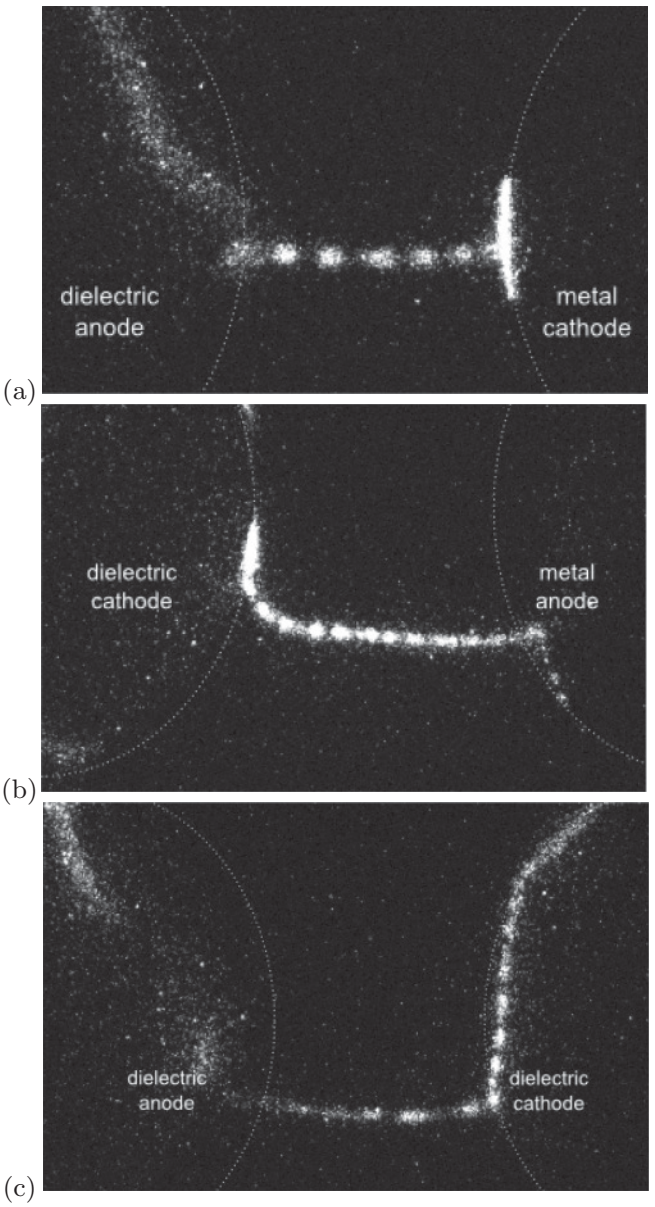

FIG. 1. Striated structures in asymmetric barrier discharges with polarities metallic cathode dielectric anode (a) and metallic anode dielectric cathode (b) as well as in a symmetric barrier discharge arrangement (c). All pictures were taken with an exposure time of 500 ns in arrangements with 1.5 mm gap at a flow rate of 150 SCCM and a voltage up to 3 $kV_{p\text{-}p}$.

P6015A and CT-1, respectively, and recorded by a Tektronix TDS 3052 oscilloscope.

The discharge atmosphere was sustained in the nonevacuated chamber with continuous argon flow of known rate flowing to the ambient air at atmospheric pressure. The flow rate of the argon gas was controlled by an MKS multi gas controller 647B. The view into the chamber was provided by a quartz glass window. Using a quartz lens, the discharge region was imaged onto the entrance slit of an ARC SpectraPro-500 monochromator with a grating of 1200. An intensified CCD (iCCD) DiCam Pro 25 SVGA camera was used in combination with a Questar QM 100BK7 far-field microscope to reveal the two-dimensional structure of a single microdischarge.

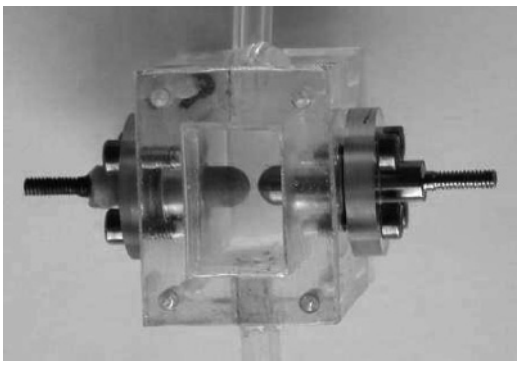

FIG. 2. Discharge cell with a gap of 1.5 mm.

Thus, every iCCD picture is a result of only one individual microdischarge event luminosity in the following figures.

III. RESULTS AND DISCUSSION

In the first part of this section, experimental results are represented and discussed. Then, a qualitative analysis of the striated microdischarge is given.

A. Experimental results

The appearance of striated structures in microdischarges depends on two basic parameters: argon flow rate and applied voltage. The argon gas purity, regulated by the flow rate, is the first important parameter. No striated structure occurred at argon flow rates below 100 SCCM, where SCCM denotes cubic centermeter per minute at standard temperature and pressure. At flow rates above 100 SCCM, no molecular nitrogen or hydroxyl radical bands comparable with the argon line intensities were detected in the optical emission spectra, as becomes obvious from Fig. 3. The argon line intensities at 763.51 nm and 750.38 nm shown in this figure correspond to the transitions of Ar I from $4p[3/2]_2$ to $4s[3/2]_2$ and $4p'[1/2]_0$ to $4s'[1/2]_1$, respectively [29,30]. The respective upper-state energies are 13.17 eV and 13.48 eV.

A quite different increase of both the upper states can be resolved as a function of the argon gas purity (flow rate). Electron impact excitation of excited (mainly the $4s$ state)

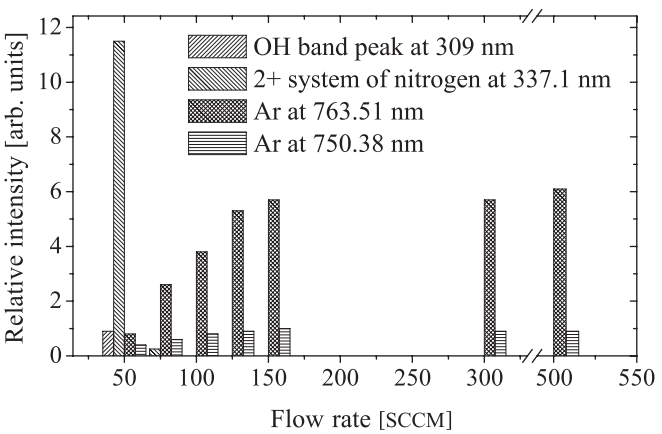

FIG. 3. Intensities of spectral lines at different argon gas flow rates.

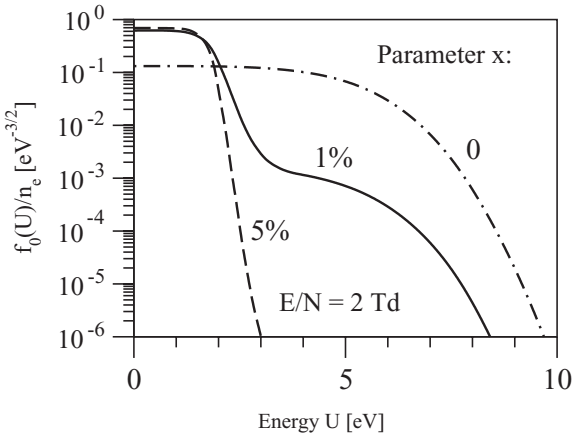

FIG. 4. Isotropic distribution $f_0(U)/n_e$ as a function of the kinetic energy U at different nitrogen admixtures x in Ar-N_2 mixtures.

atoms is the dominant volume process for the generation of the $4p[3/2]_2$ and $4p'[1/2]_0$ states of argon during the discharge phase at atmospheric pressure. The collision cross section derived, for example, from [31] for electron impact excitation of $4s$ atoms resulting in $4p[3/2]_2$ atoms is larger for all relevant energies and has a lower threshold energy than the corresponding excitation process leading to the $4p'[1/2]_0$ state. The respective rate coefficient for electron impact excitation from state i to j depends on the isotropic part f_0 of the electron velocity distribution according to

$$k_{i\to j} = \sqrt{\frac{2}{m_e}} \int_0^\infty U\, Q_{i\to j}(U) \frac{f_0(U)}{n_e} dU, \qquad (1)$$

where U, $Q_{i\to j}$, and n_e are the kinetic energy of the electrons, the collision cross section, and the density of the electrons with mass m_e, respectively.

To illustrate the impact of molecular admixtures to argon, Fig. 4 shows the isotropic distribution, normalized to the electron density, at different mixtures Ar:N_2 with the composition $(1-x)$:x for a typical value of the reduced electric field E/N of 2 Td (see discussion below). The results have been obtained from the solution of the stationary, spatially homogeneous Boltzmann equation using the solution technique given in [32] and the collision cross section data of [33] for argon and of [34] for nitrogen. Because the population of electrons with energies above 2 eV increases significantly with decreasing admixture x of nitrogen (increasing argon gas flow rate), the rate coefficients and thus the argon line intensities at 763.51 and 750.38 nm increase as well. The growth of the argon line intensity at 763.51 nm in Fig. 3 is steeper than that of the argon line intensity at 750.38 nm due to the corresponding larger collision cross sections for the stepwise excitation mentioned. The finding that the relative intensity of the 763.51 nm line is larger than that of the 750.38 nm line is in agreement with [30,35].

In order to clarify the theoretically possible influence of air or nitrogen impurities on the discharge stratification, an additional experiment in a sealed glass chamber was performed. The chamber with the same electrode setup was evacuated to high vacuum and heated to 700 K for 18 hours. After that it was filled with argon gas of purity of 99.9999%.

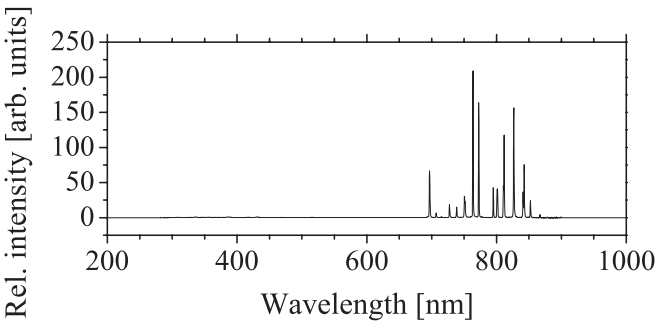

FIG. 5. Overview spectrum of the discharge in argon (99.9999% purity) in sealed system, where the striated structure was observed, too.

The overview spectrum of this discharge is shown in Fig. 5. Stratification of the discharge channel was observed in this case as well.

It has to be noted that the influence of the gas purity on the stratification of the glow discharge at low pressure has already been studied by Loudova and coworkers in [36]. Using molecular sieves, they observed only the change in the dispersion parameters in the stratified plasma channel in a neon discharge at high purity. There, the stratified structure also remained present.

In order to prevent the effect of relaxation oscillations due to negative differential conductivity [35,37–39], a high-impedance resistor was connected in addition, close to the powered electrode. The maximum known negative differential conductivity in atmospheric-pressure rare gas plasmas reaches several hundred kΩ [7,40,41]. A 2 MΩ resistor was used and striations remained. Therefore, according to the Kaufmann condition [42], an induction of the plasma channel stratification by negative differential conductivity can be excluded.

As already mentioned, the second main parameter significantly influencing the discharge behavior was the applied voltage. At the flow rate of 150 SCCM, three modes of the discharge operation could be distinguished depending on the applied voltage. The temporal evolution of the applied voltage and the discharge current corresponding to these modes are displayed in Fig. 6.

(i) First mode: Close to the burning voltage, where the applied voltage is just large enough to sustain the discharge, the first mode occurs [43]. As can be seen from Fig. 6(a), the striated discharge is present in this mode only when the metal electrode is the cathode (M−D+), while in the other half period (M+D−) the discharge appears as a normal microdischarge in the argon barrier discharge known from the literature [44]. The duration of the current pulse in the case of striated microdischarges varies between 3 and 5 μs and its amplitude does not exceed 1.5 mA. In the case of the nonstriated microdischarge, the pulse amplitude was approximately 20 mA at a pulse duration of about 500 ns.

(ii) Second mode: When increasing the applied voltage from 2 $kV_{p\text{-}p}$ to the enhanced voltage of 2.5 $kV_{p\text{-}p}$ at the flow rate of 150 SCCM, no striations appear. The shape of the discharge current peak [cf. Fig. 6(b)] takes the form of normal barrier discharges in atmospheric-pressure argon including streamer propagation [45]. It is also similar to the results reported in, for example, Ref. [44] for an argon

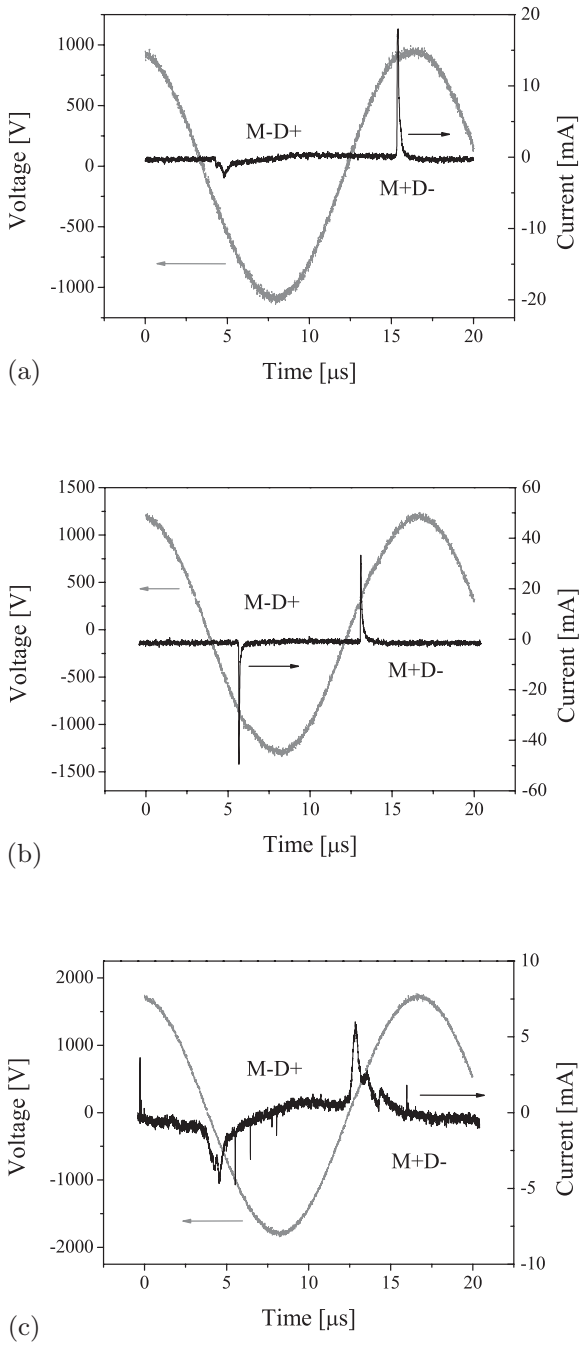

FIG. 6. Basic modes of the discharge operation in one-sided barrier discharges at atmospheric pressure in argon at a flow rate of 150 SCCM. Striated (M−D+) and nonstriated (M+D−) microdischarge at a burning voltage of 2 kV_{p-p} (a), classical microdischarges without striations during both polarities at the voltage 2.5 kV_{p-p} (b), and current pulses of striated discharges at both polarities for 4 kV_{p-p} (c).

pressure of 400 Torr, a maximum applied voltage of 2.36 kV, and a frequency of 10 kHz in a symmetric barrier discharge configuration with a gap of 2 mm. The current pulses in Fig. 6(b) have a high amplitude of 10 to 50 mA and a duration of few hundred nanoseconds.

(iii) Third mode: The third mode takes place at high overvoltage; that is, an applied peak-to-peak voltage of 4 kV in Fig. 6(c). Only striated microdischarges result during both polarities. However, these microdischarges are spatially instable and occur with disturbed structure at high flow rates.

A similar behavior with three modes depending on the applied voltage was recently observed in [46]. It is supposed that the different pre-ionization in different half periods or the inhomogeneities of the electric field on the dielectric surfaces, caused by nonuniformly deposited surface charges, locally change the electron density, resulting in different breakdowns for different voltages [46].

The transferred charge within the plasma channel (striated or nonstriated) was similar in all modes and had a value of approximately 4 nC. Due to its best temporal and spatial stability and reproducibility, the analysis has been focused on the first mode, where the striated microdischarge appears at the M−D+ polarity. Using the far-field microscope, the first two clouds of the striated column (close to the metal electrode) were visible to the naked eye. It can be concluded from this simple observation that the striated structure is spatially stable.

The experimental setup enabled the synchronous recording of the current pulse of an individual microdischarge and its iCCD picture with a given gating time. The microdischarges were not fully reproducible. However, basic characteristics of the spatial development of microdischarges and the current evolution were recognizable. Figures 7 and 8 illustrate the iCCD pictures correlated with the current measurements, which have been carried out for the first mode with the M−D+ polarity. According to the results shown in these figures, the following mechanism of discharge development is proposed. The discharge starts with a small current peak as has also been observed in [44]. In Fig. 7(a) an iCCD exposition during the first 500 ns of this small current peak is displayed, where a glow-discharge-like structure can be seen. The cathode glow, the cathode dark space, and the positive column are well pronounced. Subsequently, a plateau with a constant current of the value of about 0.20 mA above the level of the capacitive current follows [Fig. 7(b)]. During this phase, almost only the cathode layer is visible on the iCCD pictures. The striated structure appears if a second current peak (or better, current hump) develops, as becomes clear from Figs. 7(c)–7(e) and 8(a) and 8(b). The amplitude of this current hump approaches about 1.5 mA at most. Note that the diameter of the cathode layer is much larger than the constricted diameter of the plasma channel now. The striated structure vanishes with the decay of the current hump at first and the cathode layer remains until it also finally disappears.

The current onset value for the appearance of the striated structure is slightly above the plateau current value of 0.2 mA [cf. Fig. 7(b)]. However, the structures still remain at a current of 0.1 mA above the capacitive current during the current hump decay [cf. Fig. 8(b)]. This hysteresis behavior is well known from low- and medium-pressure glow discharges [6] and for the discharge constriction (with striated structure) [17] as well. It is a clear indication of nonlinear plasma processes [24,47,48].

B. Qualitative analysis of the striated microdischarge

In order to describe the observed discharge behavior qualitatively, an analysis based on the results of model calculations

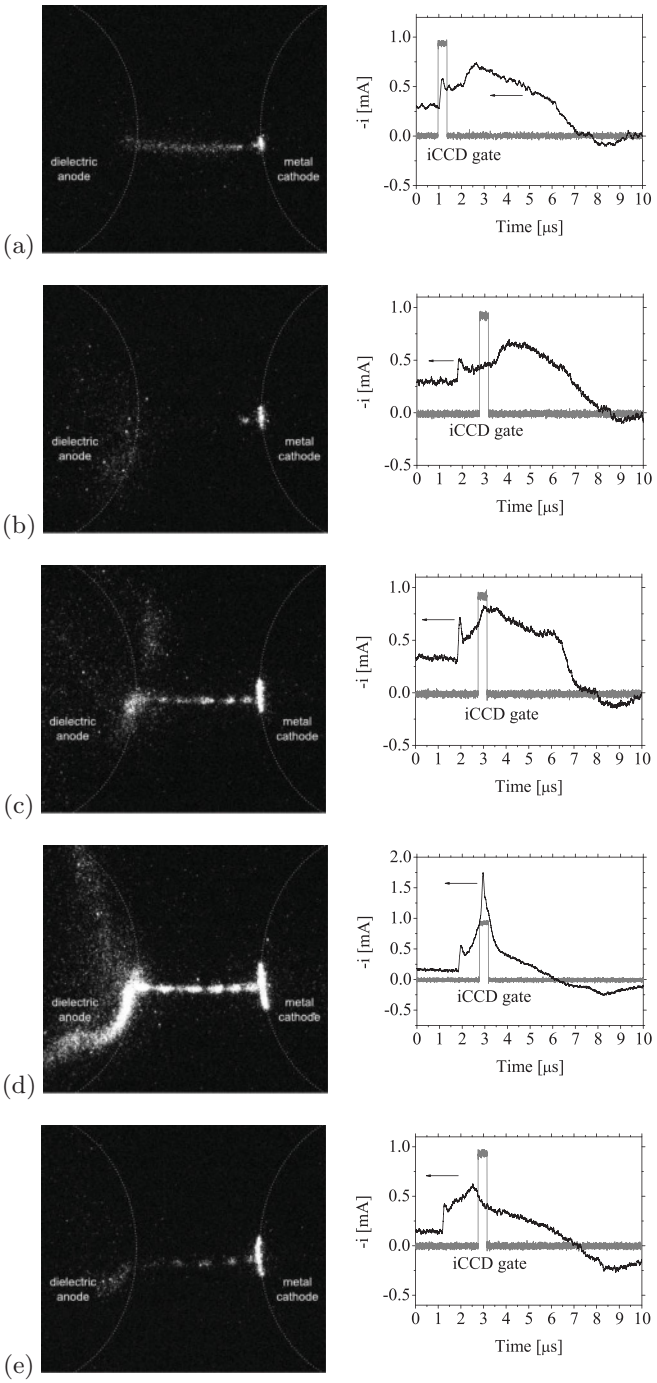

FIG. 7. Correlated iCCD and current (i) measurements at different stages of the discharge development. Argon flow rate is 150 SCCM and iCCD gate is 500 ns.

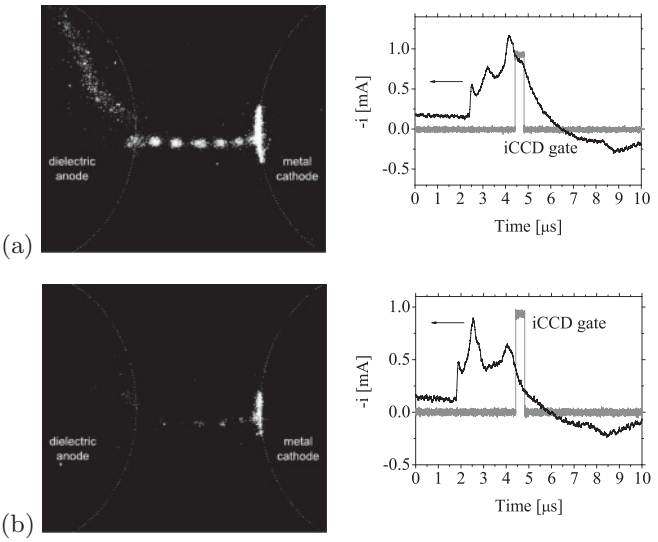

FIG. 8. Correlated iCCD and current (i) measurements at the last stage of the discharge development at conditions as in Fig. 7.

of the constriction of the positive column of dc glow discharges in argon at different pressures presented in [49] has been performed. The description of the discharges at atmospheric pressure uses, in principle, the same set of equations as that of low- and medium-pressure glow discharges, where especially three-body-collision processes have to be taken into account in the reaction kinetic model at medium and atmospheric pressure. At low and medium pressure the plasma of glow discharges can be characterized and described by means of the so-called scaling law theory [6,27,28]. Since the scaling laws were derived from the same set of equations, they have been applied to describe the observed phenomena as well. Typical scaling parameters are, for example, E/N, i/r, pr, and λ/r, where E, N, i, p, r, and λ are the electrical field, neutral gas particle concentration, current, pressure, radius of the plasma channel, and spatial wavelength of the striations, respectively.

In addition, the characteristic frequencies and lengths of the argon plasma at atmospheric pressure have been used. In Fig. 9 the lumped collision frequencies $\nu_m(U)$ and $\nu_e(U)$ for momentum and energy dissipation, the mean-free path $\lambda_m(U)$ and the energy dissipation frequency $\lambda_e(U)$ according to [50] are displayed as a function of the kinetic energy U of the electrons. These quantities have been obtained using the collision cross section data applied in [49]. Because both the dissipation frequencies for momentum and energy dissipation are larger than the frequency ω_{rf} of the applied voltage for all relevant energies [Fig. 9(a)], a quasistationary evolution of the distribution function of the electrons with respect to the energy and momentum transfer takes place. Therefore, a similarity law approach for the stable dc glow discharge has been employed in the following.

The energy dissipation length [Fig. 9(b)] considerably exceeds the mean-free path and possesses a pronounced energy dependence with substantially lower values at electron energies where inelastic collisions occur. It is directly related to the mean-free path and dissipation frequencies for momentum and energy dissipation for all energy U according to [50]

$$\lambda_e = \lambda_m \sqrt{\frac{\nu_m}{3\nu_e}}. \tag{2}$$

The comparison of λ_e and λ_m with the radius r of the plasma channel shows that a nonlocal behavior of the electron component takes place [6]. When averaging λ_e over the energy space using $f_0(U)/n_e$ obtained from the solution of the electron Boltzmann equation at $E/N = 2$ Td (see below), a mean energy dissipation length $\langle\lambda_e\rangle$ of 196 μm results. The corresponding mean electron energy is about 3.3 eV, and it

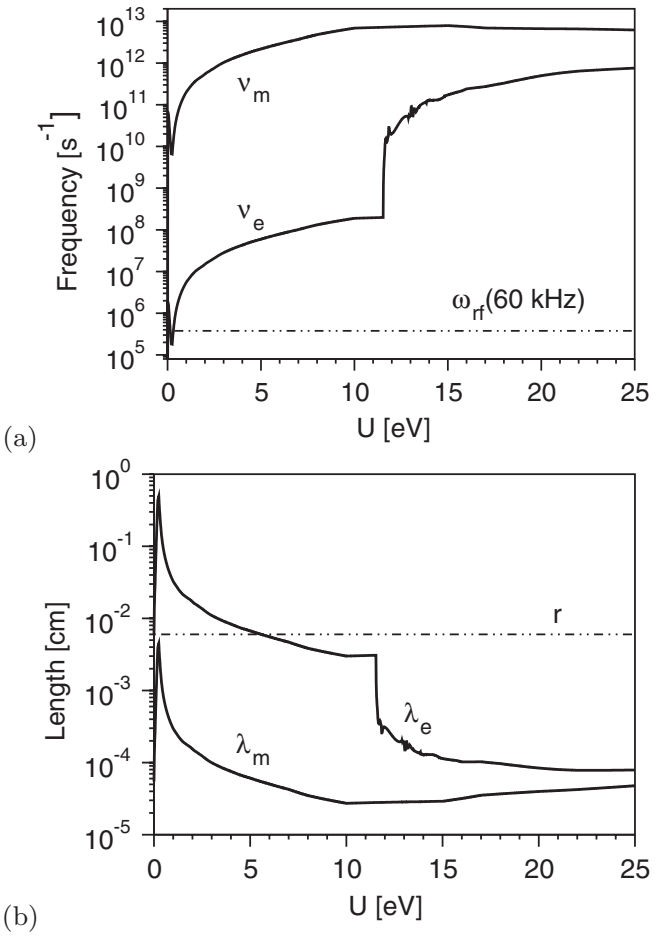

FIG. 9. Characteristic frequencies (a) and lengths (b) in argon at atmospheric pressure.

conforms to the mean energy in the transition region from glow to constricted mode obtained in [17,49].

It is known that discharges are similar if their similarity parameters coincide. Furthermore, the spatial limit of the radial discharge size in low-pressure and diffuse high-pressure discharges is determined by the dimension of the vessel (i.e., the radius of the discharge tube). However, in constricted discharges at atmospheric pressure, the radius of the discharge is determined by the plasma parameters themselves. Thus, the energy transport decreases rapidly beyond the plasma radius [49].

Based on this approach, the striated microdischarge in the first mode of the discharge operation can be described similarly to glow discharges at low and medium pressure with scaling parameters $i/r \approx 0.13$ A/cm, $pr \approx 5$ Torr cm, and $3 \leqslant \lambda/r \leqslant 5$. These values are based on the mean values of the parameters $i = 0.8$ mA, $r = 60$ μm and λ within the interval from 200 to 300 μm. Note that the estimated mean energy dissipation length $\langle\lambda_e\rangle$ is in agreement with the measured period length λ.

It is known from low-pressure discharges that probes [15] or lasers [16] trigger distortions relaxing as spatially periodic structures. The spatial distance of neighboring striations corresponds to the wavelength of the relaxing structure with periodically repeating plasma parameters. The plasma parameters, at which the transition from the diffuse to the constricted discharge form occurs, offer another possibility for triggering a particle density gradient. Spatially relaxing structures with $\lambda/r \approx 2.5$ have been observed in [17] where the structures originated at the interface between the diffuse and the constricted form of the column plasma of argon discharges at medium pressure up to 120 Torr. Such structures were also observed in comparable discharges in neon [6] with λ/r values between 1 and 6. Thus, the values of λ/r of the relaxing structures in the microdischarge investigated here ranging from 3 to 5 are in good agreement with the results reported in [6,17].

It is important to mention that the diameter of the cathode spot has a value of 120 μm and is equal to the diameter of the plasma channel in the gap during the creation of the glow regime of the microdischarge [cf. Fig. 7(a)]. However, when the striated structure develops and appears at higher current, the diameter of the cathode spot grows and reaches a value of about 0.7 mm. This result is reminiscent of the behavior of normal glow discharges at low pressure [51], where the surface current density of the cathode spot remains stable when varying the current. The observed increase of the cathode layer area at the higher current and the constant diameter of the plasma channel in the gap are accompanied by different current densities in both discharge regions. We assume, therefore, that the disturbance caused by the constriction at the transition between cathode layer at the surface and the plasma channel in the gap results in a spatial electron relaxation in which the electron density gradient in the transition area initiates the relaxation process in the plasma channel. In the course of the relaxation process resulting from that disturbance of the ionization budget, a spatially periodic electric field due to the resulting space charge densities is established [16].

In order to estimate the electric field strength in the constricted plasma column, the relation [52,53]

$$\lambda = \frac{U_{\mathrm{ex}}}{e|E_0|} \tag{3}$$

can be applied. It correlates the spatial period λ of the striations with the threshold energy U_{ex} of the lowest electron excitation process of ground-state atoms and the period-averaged electric field E_0, where e denotes the elementary charge. Using the excitation energy of the $4s[3/2]_2$ level of argon at 11.55 eV, an electric field strength between 385 and 580 V/cm is obtained corresponding to E_0/N values in the range from 1.6 to 2.4 Td. It corresponds approximately to the results in [49] for argon discharges at 500 Torr around the transition region from the diffuse to the constricted mode as well as in Ref. [6] for argon discharges at low pressure. The observed luminosity results mainly from the $4p[3/2]_2$ level of argon, which is generated mainly by electron impact excitation of the (spatially varying) $4s$ levels at atmospheric pressure.

For a more exact description of the mechanism of striation creation observed, self-consistent modeling using, for example, an approach similar to that reported in Refs. [14,16] is required. Because of the complexity of a such self-consistent approach, a study of the electron kinetics at given discharge parameters has been performed. To illustrate that the observed event is similar to the spatial electron relaxation, the spatial

evolution of the electrons in the gap region of the microdischarge, acted upon by a modulated electric field typical of striations, has been investigated applying the kinetic approach given in [54]. Using the spatially periodic electric field [55]

$$E(z) = E_0[1 + \alpha \sin(2\pi z/\lambda)], \tag{4}$$

with the period-averaged field $E_0 = -500$ V, the modulation degree $\alpha = 0.9$, and λ according to Eq. (3) for the spatial region from the metal electrode at $z = 0$ and the dielectric anode at $z = 0.15$ cm, the axially inhomogeneous Boltzmann equation of the electrons including electron-electron collisions has been solved numerically for argon gas at atmospheric pressure and a gas temperature of 300 K using the solution method described in [56]. Therefore, the Gaussian-like function

$$g(U) = \frac{i}{e\pi r^2} \frac{h(U)}{\sqrt{2/m_e}\int_0^\infty U h(U) dU/3},$$
$$h(U) = U \exp\left(-\left(\frac{U - U_c}{U_w}\right)^2\right), \tag{5}$$

with the center energy $U_c = 2$ eV and the energy width $U_w = 0.5$ eV and partial electron reflection with a probability of 80% have been employed at the metal electrode and the dielectric anode, respectively.

Figure 10 shows the resulting spatial behavior of the electron density n_e, mean energy u_e, and isotropic distribution $f_0(z,U)$ for the influx density $i/(\pi r^2) = 7$ A/cm^2 corresponding to the scaling parameters derived. The density and mean energy of the electrons vary periodically around 8.3×10^{13} cm^{-3} and 3.3 eV, respectively. Their pronounced, spatially periodic structures are mainly caused by the action of the modulated electric field under the conditions considered. The energetic backscattering of electrons by inelastic collisions with the gas atoms is of minor importance for the density and mean energy behavior, but it leads to a certain reduction of the high energy part of the distribution function illustrated in Fig. 10(b). The periodic modulation of the isotropic distribution also leads to a spatial alteration of the corresponding rate coefficients for stepwise ionization and stepwise excitation. The latter process is mainly responsible for the generation of the $4p$ and $4p'$ levels emitting the light pictured by the iCCD camera.

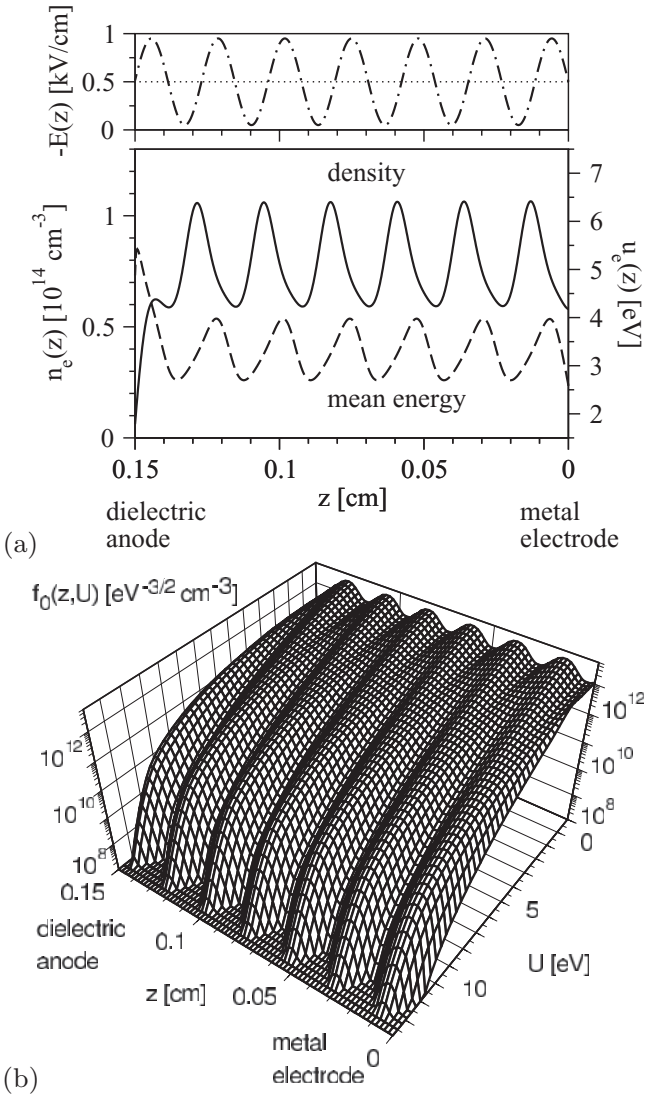

FIG. 10. Spatial evolution of the density and mean energy of the electrons (a) and of the isotropic distribution $f_0(z,U)$ (b) in argon at atmospheric pressure under the action of the periodic field (4).

IV. SUMMARY

The striated structure of microdischarges in asymmetric dielectric barrier discharges in argon at atmospheric pressure has been observed and analyzed by means of electrical measurements correlated with intensified CCD camera imaging. Depending on the applied voltage, three different modes of the discharge operation could be distinguished at argon flow rates above 100 SCCM. The main features of these modes have been given.

The first mode of the discharge operation occurring close to the burning voltage has been analyzed in more detail. It features a striated microdischarge when the metal electrode is the cathode and appears as a normal microdischarge in the barrier discharge in the other half period when the dielectric represents the cathode. The striated structures of the plasma column arise only if a second current peak develops after the occurrence of a first small current peak and of an adjacent plateau with a constant current of about 0.2 mA above the capacitive current. But it still remains afterwards for currents of about 0.1 mA above the capacitive current. This hysteresis behavior clearly indicates that nonlinear plasma processes take place.

The striated microdischarge of the first mode can be characterized as a transient atmospheric-pressure glow discharge. The application of the scaling law theory shows that it can be described by the similarity parameters $i/r \approx 0.13$ A/cm, $pr \approx 5$ Torr cm, and $3 \leqslant \lambda/r \leqslant 5$. An estimation of the spatially averaged electric field within the plasma channel leads to a reduced field strength between 1.6 and 2.4 Td. This work shows that the scaling law theory is also well applicable to transient atmospheric-pressure discharges.

The analysis of the spatially periodic luminous structure observed leads to the conclusion that they result from a spatial electron relaxation initiated by a local disturbance. The constriction of the discharge between the cathode layer and

the plasma column within the gap (electron density gradient) is assumed to be the cause of the disturbance. This finding is supported by the results obtained from kinetic studies of the electrons based on the solution of the spatially inhomogeneous electron Boltzmann equation. Spatiotemporally resolved spectroscopic measurements are intended to further clarify the mechanisms of striated microdischarges.

ACKNOWLEDGMENTS

The authors are grateful to Markus Becker for useful consultations and supplying data. This work was partly supported by the Federal German Ministry of Education and Research within project BMBF FKZ 13N9779 and FKZ 03FO1072 and by the Deutsche Forschungsgemeinschaft within SFB TR 24.

[1] A. V. Nedospasov, Sov. Phys. Usp. **11**, 174 (1968).
[2] N. L. Oleson and A. W. Cooper, Adv. Electron. Electron Phys. **24**, 155 (1968).
[3] L. Pekarek, Sov. Phys. Usp. **11**, 188 (1968).
[4] A. Garscadden, in *Gaseous Electronics*, edited by M. N. Hirsh and H. J. Oskam, Vol. 1 (Acamedic, New York, 1978), pp. 65–107.
[5] P. S. Landa, N. A. Miskinova, and Y. V. Ponomarev, Sov. Phys. Usp. **23**, 813 (1980).
[6] V. I. Kolobov, J. Phys. D **39**, R487 (2006).
[7] D. Staack, B. Farouk, A. Gutsol, and A. Fridman, Plasma Sources Sci. Technol. **17**, 025013 (2008).
[8] N. Shirai, S. Ibuka, and S. Ishii, IEEE Trans. Plasma Sci. **36**, 960 (2008).
[9] Y. Yang, J. J. Shi, J. E. Harry, J. Proctor, C. Garner, and M. G. Kong, IEEE Trans. Plasma Sci. **33**, 302 (2005).
[10] F. Iza and J. A. Hopwood, IEEE Trans. Plasma Sci. **33**, 306 (2005).
[11] G. N. Churilov, V. A. Lopatin, P. V. Novikov, and N. G. Vnukova, Instrum. Exp. Tech. **44**, 519 (2001).
[12] C. H. Yong, S. U. Han, and J. Y. Won, Appl. Phys. Lett. **93**, 051504 (2008).
[13] J. Schäfer, R. Foest, A. Ohl, and K.-D. Weltmann, Plasma Phys. Controlled Fusion **51**, 124045 (2009).
[14] S. Arndt, F. Sigeneger, H. Testrich, and C. Brandt, Plasma Chem. Plasma Process. **25**, 567 (2005).
[15] C. Brandt, H. Testrich, R. Kozakov, and C. Wilke, Rev. Sci. Instrum. **77**, 023504 (2006).
[16] F. Sigeneger and D. Loffhagen, IEEE Trans. Plasma Sci. **35**, 1260 (2007).
[17] N. A. Dyatko, Y. Z. Ionikh, I. V. Kochetov, D. L. Marinov, A. V. Meshchanov, A. P. Napartovich, F. B. Petrov, and S. A. Starostin, J. Phys. D **41**, 055204 (2008).
[18] *Non-Equilibrium Air Plasmas at Atmospheric Pressure*, edited by K. H. Becker, U. Kogelschatz, K. H. Schoenbach, and R. J. Barker (Institute of Physics Publishing, Bristol, 2005).
[19] T. Braun, J. A. Lisboa, and J. A. C. Gallas, Phys. Rev. Lett. **68**, 2770 (1992).
[20] T. Braun, J. A. Lisboa, R. E. Francke, and J. A. C. Gallas, Phys. Rev. Lett. **59**, 613 (1987).
[21] H. Shi, Y. Wang, and D. Wang, Phys. Plasmas **15**, 122306 (2008).
[22] P. Y. Cheung and A. Y. Wong, Phys. Rev. Lett. **59**, 551 (1987).
[23] P. Y. Cheung, S. Donovan, and A. Y. Wong, Phys. Rev. Lett. **61**, 1360 (1988).
[24] J. Qin, L. Wang, D. P. Yuan, P. Gao, and B. Z. Zhang, Phys. Rev. Lett. **63**, 163 (1989).
[25] J. Guikema, N. Miller, J. Niehof, M. Klein, and M. Walhout, Phys. Rev. Lett. **85**, 3817 (2000).
[26] M. Klein, N. Miller, and M. Walhout, Phys. Rev. E **64**, 026402 (2001).
[27] D. Venzke, E. Hayess, and K. Wojaczek, Contrib. Plasma Phys. **6**, 365 (1966).
[28] C. Wilke, B.-P. Koch, and B. Bruhn, Phys. Plasmas **12**, 033501 (2005).
[29] C. E. Moore, *Atomic Energy Levels*, Circular of the National Bureau of Standards 467, Vol. 1 (US Government Printing Office, Washington, DC, 1949).
[30] J. E. Sansonetti and W. C. Martin, J. Phys. Chem. Ref. Data **34**, 1559 (2005).
[31] O. Zatsarinny and K. Bartschat, J. Phys. B **37**, 4693 (2004).
[32] H. Leyh, D. Loffhagen, and R. Winkler, Comput. Phys. Commun. **113**, 33 (1998).
[33] M. Hayashi, National Institute for Fusion Science, Report No. NIFS-DATA-72 (2003).
[34] The Siglo Data base, CPAT, and Kinema Software, http://www.siglo-kinema.com.
[35] W. H. Long, W. F. Bailey, and A. Garscadden, Phys. Rev. A **13**, 471 (1976).
[36] K. Loudova and P. David, Czech. J. Phys. B **23**, 1018 (1973).
[37] Z. L. Petrovic, I. Stefanovic, S. Vrhovac, and J. Zivkovic, J. Phys. IV France **7**, 341 (1997).
[38] Z. L. Petrovic and A. V. Phelps, Phys. Rev. E **56**, 5920 (1997).
[39] S. B. Vrhovac and Z. L. Petrovic, Phys. Rev. E **53**, 4012 (1996).
[40] N. Shirai, H. Shito, S. Ibuka, and S. Ishii, Appl. Phys. Express **2**, 076001 (2009).
[41] V. I. Arkhipenko, A. A. Kirillov, Y. A. Safronau, and L. V. Simonchik, Eur. Phys. J. D **60**, 455 (2010).
[42] W. Kaufmann, Ann. Phys. (Berlin) **307**, 158 (1900).
[43] R. Brandenburg, Z. Navrátil, J. Jánský, P. St'ahel, D. Trunec, and H.-E. Wagner, J. Phys. D **42**, 085208 (2009).
[44] N. Merbahi, N. Sewraj, F. Marchal, Y. Salamero, and P. Millet, J. Phys. D **37**, 1664 (2004).
[45] P. Kloc, H.-E. Wagner, D. Trunec, Z. Navratil, and G. Fedoseev, J. Phys. D **43**, 345205 (2010).
[46] J. L. Walsch, F. Iza, N. B. Janson, V. J. Law, and M. G. Kong, J. Phys. D **43**, 075201 (2010).
[47] F. Gao, S. X. Zhao, X. S. Li, and Y. N. Wang, Phys. Plasmas **17**, 103507 (2010).
[48] G. M. Petrov and C. M. Ferreira, Phys. Rev. E **59**, 3571 (1999).
[49] M. Gnybida, D. Loffhagen, and D. Uhrlandt, IEEE Trans. Plasma Sci. **37**, 1208 (2009).
[50] R. Winkler, D. Loffhagen, and F. Sigeneger, Appl. Surf. Sci. **192**, 50 (2002).

[51] Y. P. Raizer, *Gas Discharge Physics* (Springer-Verlag, Berlin, 1997).
[52] L. D. Tsendin, Sov. J. Plasma Phys. **8**, 96 (1982).
[53] Y. B. Golubovskii, R. V. Kozakov, J. Behnke, C. Wilke, and V. O. Nekutchaev, Phys. Rev. E **68**, 026404 (2003).
[54] F. Sigeneger and R. Winkler, Plasma Chem. Plasma Process. **17**, 281 (1997).
[55] F. Sigeneger, Yu. B. Golubovskii, I. A. Porokhova, and R. Winkler, Plasma Chem. Plasma Process. **18**, 153 (1998).
[56] D. Loffhagen, Plasma Chem. Plasma Process. **25**, 519 (2005).